THE JOURNAL OF PHYSICAL CHEMISTRY Letters

Letter

pubs.acs.org/JPCL

Density and Phonon-Stiffness Anomalies of Water and Ice in the Full Temperature Range

Chang Q. Sun,*[,†,‡] Xi Zhang,[‡,§] Xiaojian Fu,[∥] Weitao Zheng,[⊥] Jer-lai Kuo,[#] Yichun Zhou,[†] Zexiang Shen,[▽] and Ji Zhou*[,∥]

[†]Key Laboratory of Low-Dimensional Materials and Application Technologies (Ministry of Education) and Faculty of Materials, Optoelectronics and Physics, Xiangtan University, Hunan 411105, China

[‡]NOVITAS, School of Electrical and Electronic Engineering, Nanyang Technological University, Singapore 639798

[§]Center for Coordination Bond and Electronic Engineering, College of Materials Science and Engineering, China Jiliang University, Hangzhou 310018, China

[∥]State Key Laboratory of New Ceramics and Fine Processing, Department of Materials Science and Engineering, Tsinghua University, Beijing 100084, China

[⊥]School of Materials Science, Jilin University, Changchun 130012, China

[#]Institute of Atomic and Molecular Sciences, Academia Sinica, Taipei 10617, Taiwan

[▽]School of Physics, Nanyang Technological University, Singapore 639798

Supporting Information

ABSTRACT: The specific-heat difference between the O:H van der Waals bond and the H−O polar-covalent bond and the Coulomb repulsion between electron pairs on adjacent oxygen atoms determine the angle−length−stiffness relaxation dynamics of the hydrogen bond (O:H−O), which is responsible for the density and phonon-stiffness oscillation of water ice over the full temperature range. Cooling shortens and stiffens the part of relatively lower specific-heat, and meanwhile lengthens and softens the other part of the O:H−O bond via repulsion. Length contraction/elongation of a specific part always stiffens/softens its corresponding phonon. In the liquid and in the solid phase, the O:H bond contracts more than the H−O elongates, hence, an O:H−O cooling contraction and the seemingly "regular" process of cooling densification take place. During freezing, the H−O contracts less than the O:H elongates, leading to an O:H−O elongation and volume expansion. At extremely low temperatures, the O:H−O angle stretching lowers the density slightly as the O:H and the H−O lengths change insignificantly. In ice, the O−O distance is longer than it is in water, resulting in a lower density, so that ice floats.

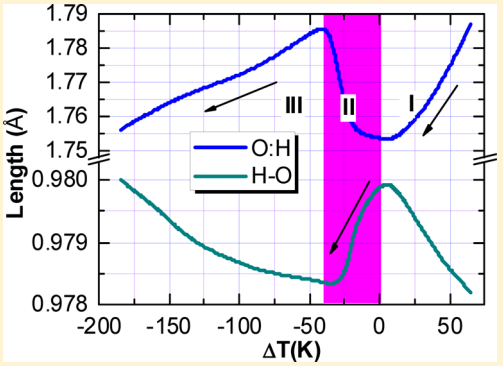

SECTION: Liquids; Chemical and Dynamical Processes in Solution

Density anomalies of water and ice and the associated angle−length−stiffness cooling relaxation dynamics of the hydrogen bond (O:H−O) continue to baffle the community, despite the intensive investigations carried out in the past decades.[1−15] Measurements[10,16,17] revealed that both the liquid and the solid H_2O undergo the seemingly regular process of cooling densification at different rates. At the water−ice transition phase, volume expansion takes place, which results in ice with a density 9% lower than the maximal density of water at 277 K.[10] At temperatures below 73 K, the density of ice drops slightly.[18]

Amazingly, the cooling densification of H_2O in the liquid and the solid phase is associated with a redshift of the high-frequency H−O phonons ($\omega_H \sim 3000$ cm^{-1}),[19] while the freezing expansion is accompanied with a blueshift of the ω_H.[20,21] Using IR spectroscopy, Medcraft et al.[22] measured the size and temperature dependence of the low-frequency O:H ($\omega_L \sim 200$ cm^{-1}) phonons in the temperature range of 4−190 K and observed that heating softens the ω_L at $T > 80$ K, but the ω_L changes insignificantly at $T < 80$ K. Earlier Raman spectroscopy[23] of bulk ice revealed that the ω_L drops monotonically within the temperature range of 25 and 272 K in addition to the resolvable fluctuations in frequency at temperatures close to 272 K.[24] However, cooperativity between the ω_L and the ω_H and the associated bond lengths remain to be understood.

The volume expansion in the freezing temperatures has been explained in terms of either the monophase of tetrahedrally coordinated structures with thermal fluctuation[3,5] or the mixed-phase of low- and high-density fragments with thermal

Received: July 3, 2013
Accepted: September 12, 2013

   dx.doi.org/10.1021/jz401380p | J. Phys. Chem. Lett. 2013, 4, 3238−3244

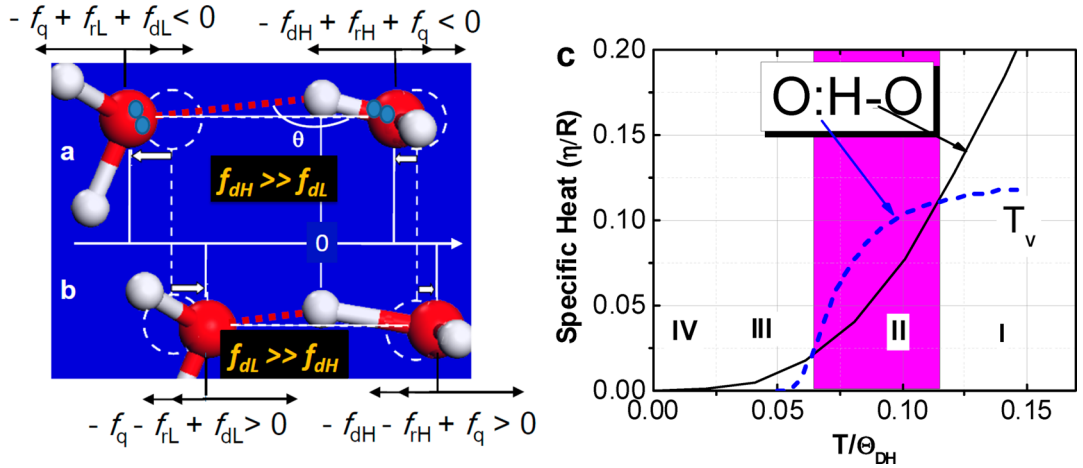

Figure 1. (a,b) Forces and relaxation dynamics of the segmented O:H−O bond and (b) the respective specific-heat of the bonding parts. Combined with the Coulomb repulsion f_q between the electron pairs of adjacent O (pairs of dots in panel a) and the resistance to deformation f_{rx} (x = H for the H−O segment with high-frequency phonons and L for the O:H segment with low-frequency phonons), the force due to cooling contraction (related to the specific heat) f_{dx} drives the two parts to relax in the same direction but by different amounts. H atom is the reference origin. (c) Because of the difference in their Debye temperatures (Table 1), the specific heat η_L of the O:H rises faster toward saturation than the η_H. Such a specific-heat decomposition results in three regions that correspond, respectively, to the phases of liquid (I), solid (III), and liquid−solid transition (II) with different specific-heat ratios. At extremely low temperatures (IV), $\eta_L \approx \eta_H \approx 0$. R is the gas constant. (The η_L in the solid phase differs from the η_L in the liquid, which does not influence the validity of the hypothesis).

modulation of the fragmental ratios.[25,26] However, little attention has been paid to the mechanism for the seemingly regular process of cooling densification in both the liquid and the solid phase or to the mechanism for the slight drop in density at extremely low temperatures. Therefore, a consistent understanding of the mechanism behind the density and phonon-stiffness relaxation anomalies of water and ice in the full temperature range is greatly desirable.

This Letter reports the latest progress. Based on the framework of O:H−O bond specific-heat disparity, Raman spectroscopy measurements, and molecular dynamics (MD) calculations of the hydrogen bond angle−length−stiffness relaxation of water/ice over the full temperature range, we have been able to reconcile the measured mass-density[10] and Raman-frequency transitions of water/ice. The specific-heat disparity between the O:H and the H−O of the O:H−O bond and the Coulomb repulsion between the electron pairs of the adjacent oxygen atoms (O−O) are shown to be the key to resolving the density and phonon-stiffness puzzles.

We consider the basic structural unit of $O^{\delta-}$:$H^{\delta+}$−$O^{\delta-}$ (also denoted as "O···H−O") to represent the $O^{\delta-}$—$O^{\delta-}$ interactions in H_2O, except for H_2O under extremely high pressures and temperatures.[27] The fraction δ represents the polarity of the $H^{\delta+}$−$O^{\delta-}$ polar-covalent bond. Figure 1a illustrates the O:H−O bond and forces acting on O atoms. The pair of dots on the O in the left represents the nonbonding lone pair ":". The lone pair belongs to the sp^3-orbit hybridized oxygen. The pair of dots on the right represents the bonding electron pair "−". The bonding pair is shared by the H−O polar-covalent bond and centered at sites close to oxygen. The H atom serves as the point of reference in the O:H−O system. For completeness, we define the entire hydrogen bond to be O:H−O, the intramolecular polar-covalent bond as the H−O bond and the intermolecular van der Waals (vdW) bond as the O:H bond hereon.[28]

A hydrogen bond is comprised of the O:H bond (dashed lines) and the H−O bond rather than either of them alone.[24,28] The H−O bond is much shorter, stronger, and stiffer than the O:H bond (comparison shown in Table 1). The O:H bond breaks at the evaporating point (T_v) of water (373 K).[29]

Table 1. Summary of the Segmental Length d_x, Strength E_x (Energy), Debye Temperature Θ_{Dx},[31,32] Stiffness ω_x (Vibration Frequency), Melting Point T_{mx}, and the Inter-Atomic and Inter-Electron-Pair Interactions of the O:H−O Bond Compared with Those of the C−C Bond in a Diamond[30]

segment (x)	d_x (nm)	E_x(eV)	ω_x (cm^{-1})	Θ_{Dx} (K)	T_{mx}(K)	interaction
H−O	~0.10	~4.00	>3000	>3000	-	exchange
O:H	~0.17	>0.10	~200	198	273	van der Waals
O−O	-	-	-	-	-	Coulomb repulsion
C−C	0.15	1.84	1331	2230	3800	exchange

However, the H−O bond is much harder to break as the bond energy of ~4.0 eV is twice that of the C−C bond in diamond (1.84 eV).[30]

The Coulomb repulsion between the electron pairs of adjacent O−O is the key to the O:H−O bond relaxation under excitation.[24,28] Combined with the forces of the Coulomb repulsion, f_q, resistance to O dislocation, f_{rx} (x = H for the H−O and L for the O:H bond), the force due to cooling contraction (related to the respective specific heat of the segment), f_{dx}, drives these two segments to relax in the same direction but by different amounts.

Generally, the specific heat is regarded as a macroscopic quantity integrated over all bonds of the system, which is the amount of energy required to raise the temperature of the substance by 1 K. However, in dealing with the representative (or average) for all bonds of the entire specimen, one has to consider the specific heat per bond that is obtained by dividing the bulk specific heat by the total number of bonds involved. In the case of the O:H−O bond, we need to consider the specific heat η_x characteristics of the two segments separately (see

dx.doi.org/10.1021/jz401380p | J. Phys. Chem. Lett. 2013, 4, 3238−3244

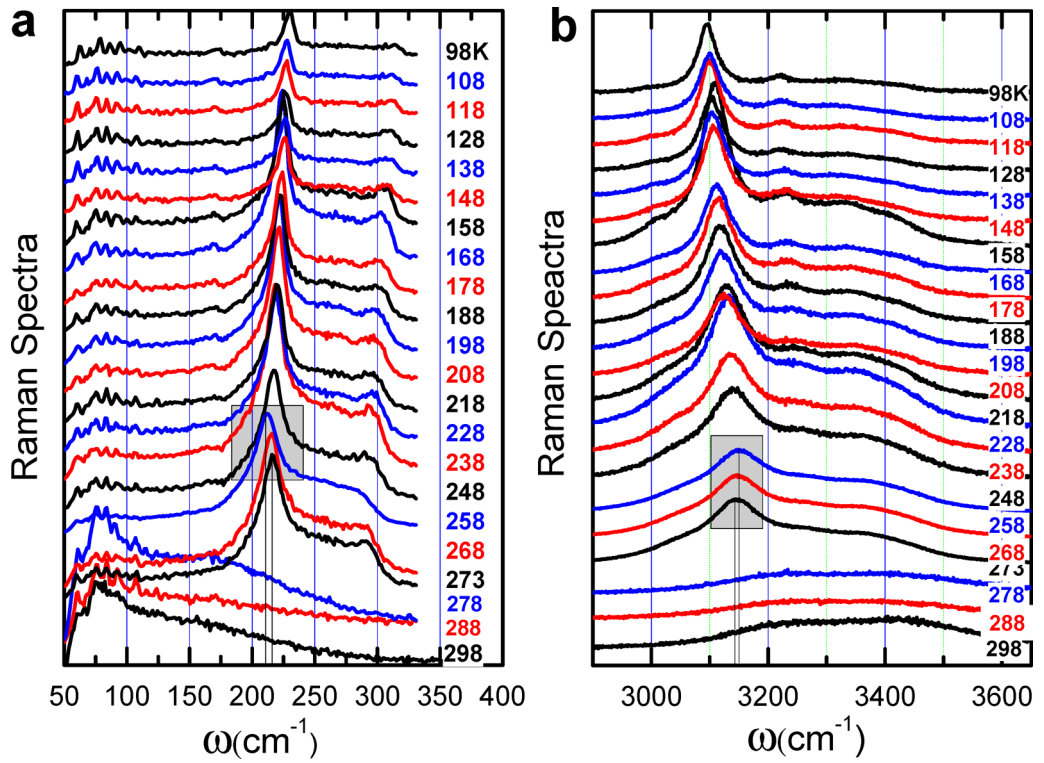

Figure 2. Temperature-dependent Raman shifts of (a) ω_L (the O:H stretching phonon) and (b) ω_H (H−O stretching mode) show three regions of the liquid I (T > 273 K), solid III (T < 258 K), and the freezing II (258−273 K) phases. Region IV is out of the temperature scope of liquid nitrogen.

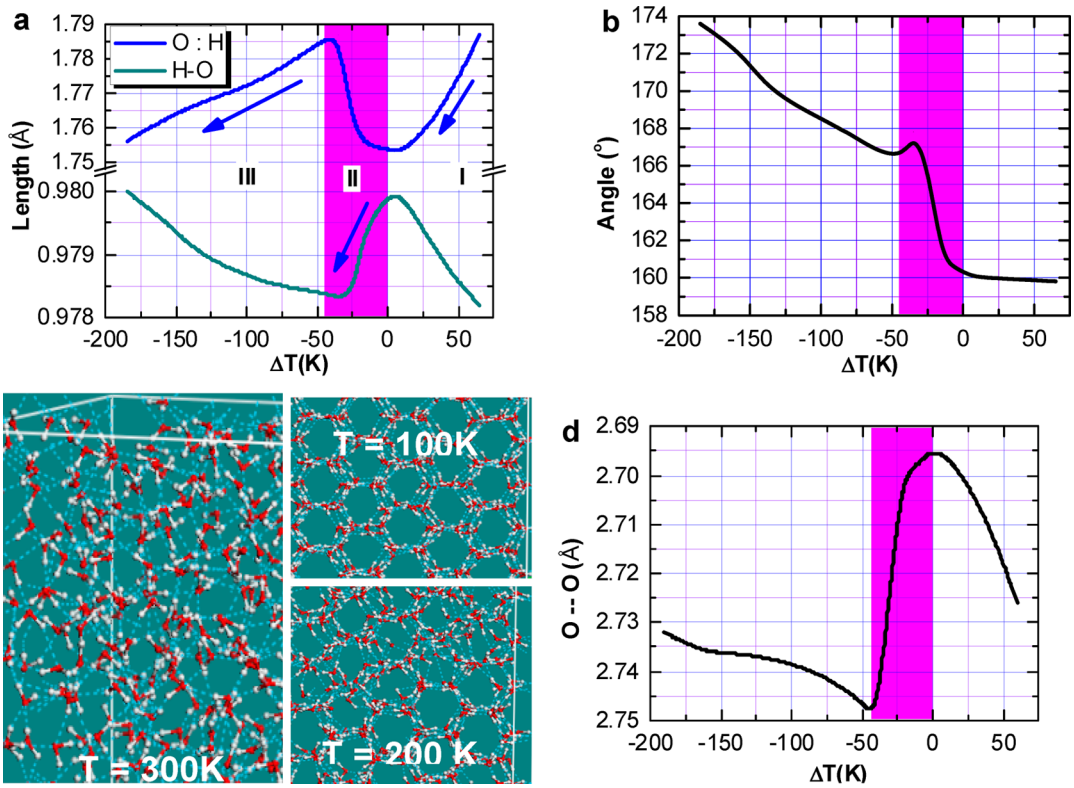

Figure 3. MD derivatives of (a) the cooperative length relaxation of the O:H and the H−O part of the O:H−O bond in the phases of liquid (I), solid (III), and liquid−solid transition (II). Arrows denote the cooling contraction of the master segments, which are coupled with the expansion of the slaves. $\Delta T = T - T_{max}$ with T_{max} = 277 K is the maximal density temperature. (b) O:H−O bond angle widening driven by cooling also exhibits three regions. (c) Snapshots of the MD trajectory show that the V-shaped H−O−H molecules remain intact at 300 K because of the robustness of the H−O bond (∼4.0 eV/bond) with pronounced quantum fluctuations in the angle and in the d_L in liquid phase. (d) The change of the O−O distance agrees with the measured three-region water and ice densities.[10] In ice, the O−O distance is longer than that in water, which results in ice floating.

dx.doi.org/10.1021/jz401380p | J. Phys. Chem. Lett. 2013, 4, 3238−3244

Figure 1c) because of the difference in their strengths. The Debye temperature Θ_{Dx} determines the slope of the specific-heat curve while the cohesive energy of the bond E_x determines the integral of the specific-heat curve from 0 K to the melting point T_{mx}.[33] The specific-heat curve of the segment with a relatively lower Θ_{Dx} value will rise to saturation faster than the other segment. The Θ_{Dx}, which is lower than the T_{mx}, is proportional to the characteristic frequency of the vibration (ω_x) of the segment. Thus, we have the following relations (see Table 1):

$$\begin{cases} \Theta_{DL}/\Theta_{DH} \approx 198/\Theta_{DH} \\ \qquad\quad \approx \omega_L/\omega_H \\ \qquad\quad \approx 200/3000 \sim 1/15 \\ (\int_0^{T_{mH}} \eta_H \, dt)/(\int_0^{T_{mL}} \eta_L \, dt) \\ \quad \approx E_H/E_L \approx 4.0/0.1 \sim 40 \end{cases} \tag{1}$$

Such a specific-heat disparity between the O:H and the H−O segments creates four temperature regions with different η_L/η_H ratios, which should correspond to the phases of liquid (I), solid (III), and liquid−solid transition (II). In region IV, $\eta_L \approx \eta_H \approx 0$. The crossing points correspond to the density extremes. This specific-heat curve applies to the entire temperature range for the liquid and the solid phase, as Raman shift showed the monotonic change in the liquid phase.[17]

The consistency in the number of temperature regions (i.e., phases I, II, III, IV) of the proposed specific-heat curve (Figure 1c), the mass-density transition (see Supporting Information, SI),[10,23] Raman phonon relaxation,[20−22,29] and the O:H−O bond angle−length−stiffness relaxation dynamics (Figure 2 and Figure 3) suggest that the segment with a relatively lower specific heat is thermally more active than the other segment. This thermally active segment serves as the "master" that undergoes cooling contraction (or thermal expansion) while forcing the other "slave" segment to elongate (or contract) through Coulomb repulsion. Therefore, as can be derived from Figure 1c, the specific-heat ratio, the master segment, and the O−O length change in each temperature region are correlated.

Pairing up the forces in each of the (a) and (b) cases,

$$\left.\begin{matrix} -f_q + f_{rL} + f_{dL} \\ -f_{dH} + f_{rH} + f_q \end{matrix}\right\} \begin{matrix} < 0 \quad (a) \\ > 0 \quad (b) \end{matrix}$$

one has,

$$\begin{cases} f_{dH} - (f_{rL} + f_{dL} + f_{rH}) > 0 \quad (a) \\ f_{dL} - (f_{rL} + f_{dL} + f_{rH}) > 0 \quad (b) \end{cases}$$

Serving as the master segment, the H−O bond in (a) contracts less than the O:H elongates; however, the O:H bond in (b) contracts more than the H−O elongates. The specific-heat difference between the two segments results in the relaxation of the O:H and the H−O bond in different regions in the following way upon H_2O being cooled,

$$\left.\begin{matrix} \text{II} & (\eta_H < \eta_L): & f_{dH} > (f_{dL} + f_{rL} + f_{rH}) \\ \text{I, III} & (\eta_L < \eta_H): & f_{dL} > (f_{dH} + f_{rL} + f_{rH}) \\ \text{Transition} & (\eta_L = \eta_H): & f_{dH} = f_{dL} \end{matrix}\right\}$$
$$\Rightarrow \Delta d_{O-O} \Rightarrow (\Delta V)^{1/3} \begin{Bmatrix} > \\ < \\ = \end{Bmatrix} 0 \tag{2}$$

Because of the repulsion and the strength difference between the segments,[24] the length of the softer O:H bond always relaxes more than that of the stiffer H−O bond in the same direction: $|\Delta d_L| > |\Delta d_H|$. Thus, we expect that the O:H−O bond relaxes cooperatively in the following manner during cooling:

(i) In the transition phase (II), $\eta_H < \eta_L$ and $f_{dH} \gg f_{dL}$, H−O bond contraction dominates. The stiffer H−O bond contracts less than the O:H bond elongates, resulting in $\Delta d_{O-O} = \Delta d_L - \Delta d_H > 0$. Therefore, a net O−O length gain and an accompanying volume expansion ($\Delta V > 0$) takes place.

(ii) In the liquid (I) and solid (III) phases, $\eta_L < \eta_H$ and $f_{dL} \gg f_{dH}$. The master and the slave swap roles. The softer O:H bond contracts significantly more than the H−O bond elongates, $\Delta d_{O-O} = \Delta d_H - \Delta d_L < 0$. Hence, a net O−O contraction results in a gain in the mass density.

(iii) At the crossing points, $\eta_H = \eta_L$ and $f_{dH} \gg f_{dL}$. There is a transition between O−O expansion and contraction, corresponding to the density maximum at 277 K or the density minimum below the freezing point.[10,13]

(iv) Meanwhile, the repulsion increases the O:H−O angle θ and polarizes the electron pairs during relaxation. At extremely low temperatures (IV), d_x changes insignificantly, but the θ continues relaxation.

A segment increases in stiffness as it becomes shorter, while the opposite occurs as it elongates.[24,28,34] The Raman shift, which is proportional to the square root of bond stiffness, directly approximates the length and strength change of the bond during relaxation. Comparing the energy of a vibration system to the Taylor series of the interatomic potential energy, $u_x(r)$, leads to the dimensionality of the vibration (phonon) frequencies:[28]

$$\Delta\omega_x \propto \left(\frac{\partial^2 u_x(r)}{\mu \partial r^2}\bigg|_{r=d_x} \right)^{1/2} \propto \sqrt{E_x/\mu}\,/d_x \propto \sqrt{Y_x d_x} \tag{3}$$

The stiffness is the product of the Young's modulus ($Y_x \propto E_x/d_x^3$) and the length of the segment in question.[24] The μ is the reduced mass of the vibrating dimer. Therefore, the Raman shift directly measures the segmental stiffness based on the dimensionality analysis.

In order to verify our hypotheses and predictions regarding the O:H−O bond angle−length−stiffness change, the specific-heat disparity, and the density and phonon-frequency anomalies of water and ice, we conducted Raman measurements and MD calculations as a function of temperature. Raman measurements of 0.5 g deionized water poured on a silica stage were conducted using the Lab RAM HR800 Raman spectrometer (HORIBA Jobin Yvon Ltd.) with a 632.8-nm He−Ne laser as the light source. Semiconductor refrigeration-cooling detection systems were used to collect the data at the programmable controlled temperatures at the ambient pressure. The frequency range was set to 50−1000 and 2600−4000

dx.doi.org/10.1021/jz401380p | J. Phys. Chem. Lett. 2013, 4, 3238−3244

cm^{-1}. The temperature was lowered from 298 to 98 K at a rate of 3 K/min rate, using a 10-K step size (some measurements were carried out at 5-K step size). Each spectrum is an accumulation of four scans, and each scan took 30 s. At each step, the measurement was conducted after the temperature had been stabilized for 5 min. Two MD computational methods were used in examining the mono- and the mixed-phase models based on the relaxation of the Ih supercells containing 360 H_2O molecules. More details of the calculation procedures are described in the Supporting Information.

The measured Raman spectra in Figure 2 show three regions: $T > 273$ K (I), $273 \geq T \geq 258$ K (II), and $T < 258$ K (III), which are in accordance with the MD calculations (SI) and predictions:

(i) At $T > 273$ K (I), abrupt shifts of the ω_L from 75 to 220 cm^{-1} and the ω_H from 3200 to 3140 cm^{-1} indicate ice formation. The cooperative ω_L blueshift and ω_H redshift indicate that cooling shortens and stiffens the O:H bond but lengthens and softens the H−O bond in the liquid phase, which confirms the predicted master role of the O:H bond in liquid water. This conclusion applies to $T <$ 363 K (see Figure S2 Raman spectra in SI).

(ii) At $T < 258$ K (III), the trend of phonon relaxation remains as it is in the region of $T > 273$ K despite a change in the relaxation rates. Cooling from 258 K stiffens the ω_L from 215 to 230 cm^{-1} and softens the ω_H from 3150 to 3100 cm^{-1}. Other supplementary peaks at ∼300 and ∼3400 cm^{-1} change insignificantly. The cooling softening of the ω_H mode agrees with that measured using IR spectroscopy[35] of ice clusters of 8−150 nm sizes. When the temperature drops from 209 to 30 K, the ω_H shift from 3253 to 3218 cm^{-1}. For clusters of 5 nm size or smaller, the ω_H is stiffened by an addition of 40 cm^{-1}.

(iii) At 273−258 K (II), situation reverses. Cooling shifts the ω_H from 3140 to 3150 cm^{-1} and the ω_L from 220 to 215 cm^{-1}; see the shaded areas. Agreeing with the Raman ω_H shift measured in the temperature range around 273 K,[20,21] the cooperative shift of the ω_H and the ω_L confirms the exchange in the master and slave role of the O:H and the H−O bond during freezing.

Figure 3 shows the MD-derived relaxation of (a) the segmental lengths, (b) the O:H−O bond angle θ, (c) the snapshots of the MD trajectory, and (d) the O−O distance as a function of temperature. As shown in Figure 3a, the shortening of the master segments (denoted with arrows) is always coupled with a lengthening of the slaves during cooling. The temperature range of interest consists of three regions: in the liquid region I and the solid region III, the O:H bond contracts significantly more than the H−O bond elongates, resulting in a net loss of the O−O length. Thus, cooling-driven densification of H_2O happens in both the liquid and the solid phase. This mechanism differs completely from the mechanism conventionally adopted for the standard cooling densification of other regular materials in which only one kind of chemical bond is involved.[36] By contrast, in the transition phase II,[10,12,13] the master and the slave swap roles. The O:H bond elongates more than the H−O bond shortens so that a net gain in the O−O length occurs.

The θ angle widening (Figure 3b) contributes to the volume change. In the liquid phase I, the mean θ valued at 160° remains almost constant. However, the snapshots of the MD trajectory in Figure 3c and the MD movie in the SI show that the V-shaped H−O−H molecules remain intact at 300 K over the entire duration recorded. This configuration is accompanied by high fluctuations in the θ and the d_L in this regime, which indicates the dominance of tetrahedrally coordinated water molecules.[37] In region II, cooling widens the θ from 160° to 167°, which contributes a maximum of +1.75% to the O:H−O bond elongation and ∼5.25% to volume expansion. In phase III, the θ increases from 167° to 174°, and this trend results in a maximal value of −2.76% to the volume contraction. An extrapolation of the θ enlargement in Figure 3b results in the O−O distance lengthening, which explains the slight drop in density and the steady ω_L (d_L and E_L) observed at extremely low temperatures.[22,23]

The calculated temperature dependence of the O−O distance shown in Figure 3d matches satisfactorily with that of the measured density profile.[10,16] Importantly, the O−O distance is longer in ice than it is in water, and therefore, ice floats.

The MD-movie (SI) shows that in the liquid phase, the H and the O attract each other between the H:O but the O−O repulsion prevents this occurrence. The intact O−H−O motifs are moving restlessly because of the high fluctuation and frequent switching of the H:O interactions. Furthermore, the cooperative ω_L and ω_H shifts provide further evidence for the persistence of the Coulomb repulsion between the bonding and the nonbonding electron pairs in liquid. The presence of the electron lone pair results from the sp^3-orbit hybridization of oxygen that tends to form tetrahedral bonds with its neighbors.[37] Therefore, the H_2O in the bulk form of liquid could possess the tetrahedrally coordinated structures with thermal fluctuation.[5] Snapshots of the MD trajectory revealed little discrepancy between the mono- and the mixed-phase structural models (see SI).

The current understanding may extend to the following important findings. One is the negative thermal expansion (NTE) in other materials, and the other is the salt stiffening of the high-frequency Raman phonons of liquid water.

The NTE happens to graphite,[38] graphene oxide paper,[39] $ZrWO_3$,[40,41] and other compounds composed of N, F, and O at various temperatures as summarized in ref 42. The observed NTE shares the same feature of water at freezing (see Figure S1 in the SI). The current understanding indicates that the NTE results from the involvement of at least two kinds of short-range interactions and the associated specific-heat disparity between bonds of different interactions. For graphite instances, the (0001) intralayer covalent bond and the interlayer van der Vaals bond interactions may take the respective role. O, N, and F create lone pair of electrons upon reaction.

An addition of cations and anions can modulate the surface tension of water and the ability of water dissolving proteins, known as the Hofmeister mysteries.[43,44] Adding salt (NaCl,[45] NaBe,[46] LiCl,[47] $NaClO_4$, and $Mg(ClO_4)_2$[48,49]) into liquid water not only lowers the dissociation energy of the O:H bond but also stiffens the high-frequency H−O phonons, which shares the same attribute of the heating effect on H−O vibration.[29,45] The replacement of O ions with ions of salts, acids, or sugars and heating could weaken the Coulomb repulsion between the charged ions. The reduced/enhanced repulsion may modulate the Coulomb repulsion. Further investigation from the perspective of "specific heat disparity between the short-range interactions" and "Coulomb interaction modulation" for these phenomena would be even more fascinating and revealing.

The proposed mechanisms for (i) the seemingly regular processes of cooling densification of the liquid and the solid H_2O, (ii) the abnormal freezing expansion, (iii) the floating of ice, and, (iv) the four-region O:H−O bond angle−length−stiffness relaxation dynamics of water and ice have been justified. Agreement between MD calculations and the measured mass-density[10] and phonon-frequency relaxation dynamics in the temperature range of interest has verified our hypotheses and predictions:

(i) Interelectron-pair Coulomb repulsion and the segmental specific-heat disparity of the O:H−O bond determine the change in its angle, length, stiffness and the density and the phonon-frequency anomalies of water ice.

(ii) The segment with a relatively lower specific-heat serves as the master to contract and drive the O:H−O bond cooling relaxation. The softer O:H bond always relaxes more in length than the stiffer H−O bond does in the same direction. The cooling widening of the O:H−O angle contributes positively to the volume expansion at freezing and at extremely low temperatures.

(iii) In the liquid and the solid phase, the O:H bond contracts more than the H−O bond elongates, resulting in the cooling densification of water and ice, which is completely different from the process experienced by other regular materials.

(iv) In the freezing transition phase, the H−O bond contracts less than the O:H bond lengthens, resulting in expansion during freezing. The O−O distance is larger in ice than it is in water, and therefore, ice floats.

(v) The segment increases in stiffness as it shortens, while the opposite occurs as it elongates. The density variation of water ice is correlated to the cooperative O:H and H−O length and phonon-stiffness relaxation dynamics.

■ ASSOCIATED CONTENT

Ⓢ Supporting Information

Details of the tetrahedrality of water interactions and methodologies as well as nomenclatures regarding basic concepts published previously but not covered in the main text. An MD movie showing the thermal fluctuation of water molecules at 300 K is also available. This material is available free of charge via the Internet at http://pubs.acs.org.

■ AUTHOR INFORMATION

Corresponding Authors

*E-mail: ecqsun@ntu.edu.sg

*E-mail: zhouji@tsinghua.edu.cn.

Notes

The authors declare no competing financial interest.

■ ACKNOWLEDGMENTS

Special thanks to Phillip Ball, Yi Sun, Buddhudu Srinivasa, and John Colligon for their critical readings and helpful discussions. Financial support received from NSF (Nos.: 21273191, 1033003, and 90922025) China is gratefully acknowledged.

■ REFERENCES

(1) Clark, G. N. I.; Cappa, C. D.; Smith, J. D.; Saykally, R. J.; Head-Gordon, T. The Structure of Ambient Water. *Mol. Phys.* **2010**, *108*, 1415.

(2) Soper, A. K.; Teixeira, J.; Head-Gordon, T. Is Ambient Water Inhomogeneous on the Nanometer-Length Scale? *Proc. Natl. Acad. Sci. U.S.A.* **2010**, *107*, E44.

(3) Head-Gordon, T.; Johnson, M. E. Tetrahedral Structure or Chains for Liquid Water. *Proc. Natl. Acad. Sci. U.S.A.* **2006**, *103*, 7973.

(4) Clark, G. N.; Hura, G. L.; Teixeira, J.; Soper, A. K.; Head-Gordon, T. Small-Angle Scattering and the Structure of Ambient Liquid Water. *Proc. Natl. Acad. Sci. U.S.A.* **2010**, *107*, 14003.

(5) Petkov, V.; Ren, Y.; Suchomel, M. Molecular Arrangement in Water: Random but Not Quite. *J. Phys.: Condens. Matter* **2012**, *24*, 155102.

(6) Stone, A. J. Water from First Principles. *Science* **2007**, *315*, 1228.

(7) Stokely, K.; Mazza, M. G.; Stanley, H. E.; Franzese, G. Effect of Hydrogen Bond Cooperativity on the Behavior of Water. *Proc. Natl. Acad. Sci. U.S.A.* **2010**, *107*, 1301.

(8) Huang, M. Y.; Yan, H. G.; Chen, C. Y.; Song, D. H.; Heinz, T. F.; Hone, J. Phonon Softening and Crystallographic Orientation of Strained Graphene Studied by Raman Spectroscopy. *Proc. Natl. Acad. Sci. U.S.A.* **2009**, *106*, 7304.

(9) English, N. J.; Tse, J. S. Density Fluctuations in Liquid Water. *Phys. Rev. Lett.* **2011**, *106*, 037801.

(10) Mallamace, F.; Branca, C.; Broccio, M.; Corsaro, C.; Mou, C. Y.; Chen, S. H. The Anomalous Behavior of the Density of Water in the Range 30 K < *T* < 373 K. *Proc. Natl. Acad. Sci. U.S.A.* **2007**, *104*, 18387.

(11) Mallamace, F.; Broccio, M.; Corsaro, C.; Faraone, A.; Majolino, D.; Venuti, V.; Liu, L.; Mou, C. Y.; Chen, S. H. Evidence of the Existence of the Low-Density Liquid Phase in Supercooled, Confined Water. *Proc. Natl. Acad. Sci. U.S.A.* **2007**, *104*, 424.

(12) Mishima, O.; Stanley, H. E. The Relationship between Liquid, Supercooled and Glassy Water. *Nature* **1998**, *396*, 329.

(13) Moore, E. B.; Molinero, V. Structural Transformation in Supercooled Water Controls the Crystallization Rate of Ice. *Nature* **2011**, *479*, 506.

(14) Molinero, V.; Moore, E. B. Water Modeled as an Intermediate Element between Carbon and Silicon. *J. Phys. Chem. B* **2009**, *113*, 4008.

(15) Wang, C.; Lu, H.; Wang, Z.; Xiu, P.; Zhou, B.; Zuo, G.; Wan, R.; Hu, J.; Fang, H. Stable Liquid Water Droplet on a Water Monolayer Formed at Room Temperature on Ionic Model Substrates. *Phys. Rev. Lett.* **2009**, *103*, 137801.

(16) Erko, M.; Wallacher, D.; Hoell, A.; Hauss, T.; Zizak, I.; Paris, O. Density Minimum of Confined Water at Low Temperatures: A Combined Study by Small-Angle Scattering of X-rays and Neutrons. *Phys. Chem. Chem. Phys.* **2012**, *14*, 3852.

(17) Suzuki, H.; Matsuzaki, Y.; Muraoka, A.; Tachikawa, M. Raman Spectroscopy of Optically Levitated Supercooled Water Droplet. *J. Chem. Phys.* **2012**, *136*, 234508.

(18) Rottger, K.; Endriss, A.; Ihringer, J.; Doyle, S.; Kuhs, W. F. Lattice-Constants and Thermal-Expansion of H_2O and D_2O Ice I*h* between 10 and 265 K. *Acta Crystallogr. B* **1994**, *50*, 644.

(19) Yoshimura, Y.; Stewart, S. T.; Mao, H. K.; Hemley, R. J. In Situ Raman Spectroscopy of Low-Temperature/High-Pressure Transformations of H_2O. *J. Chem. Phys.* **2007**, *126*, 174505.

(20) Durickovic, I.; Claverie, R.; Bourson, P.; Marchetti, M.; Chassot, J. M.; Fontana, M. D. Water-Ice Phase Transition Probed by Raman Spectroscopy. *J. Raman Spectrosc.* **2011**, *42*, 1408.

(21) Xue, X.; He, Z.-Z.; Liu, J. Detection of Water-Ice Phase Transition Based on Raman Spectrum. *J. Raman Spectrosc.* **2013**, *44*, 1045.

(22) Medcraft, C.; McNaughton, D.; Thompson, C. D.; Appadoo, D.; Bauerecker, S.; Robertson, E. G. Size and Temperature Dependence in the Far-IR Spectra of Water Ice Particles. *Astrophys. J.* **2012**, *758*, 17.

(23) Johari, G. P.; Chew, H. A. M.; Sivakumar, T. C. Effect of Temperature and Pressure on Translational Lattice Vibrations and Permittivity of Ice. *J. Chem. Phys.* **1984**, *80*, 5163.

(24) Sun, C. Q.; Zhang, X.; Zheng, W. T. Hidden Force Opposing Ice Compression. *Chem. Sci.* **2012**, *3*, 1455.

(25) Huang, C.; Wikfeldt, K. T.; Tokushima, T.; Nordlund, D.; Harada, Y.; Bergmann, U.; Niebuhr, M.; Weiss, T. M.; Horikawa, Y.; Leetmaa, M.; Ljungberg, M. P.; Takahashi, O.; Lenz, A.; Ojamäe, L.; Lyubartsev, A. P.; Shin, S.; Pettersson, L. G. M.; Nilsson, A. The Inhomogeneous Structure of Water at Ambient Conditions. *Proc. Natl. Acad. Sci. U.S.A.* **2009**, *106*, 15214.
(26) Wernet, P.; Nordlund, D.; Bergmann, U.; Cavalleri, M.; Odelius, M.; Ogasawara, H.; Naslund, L. A.; Hirsch, T. K.; Ojamae, L.; Glatzel, P.; Pettersson, L. G. M.; Nilsson, A. The Structure of the First Coordination Shell in Liquid Water. *Science* **2004**, *304*, 995.
(27) Wang, Y.; Liu, H.; Lv, J.; Zhu, L.; Wang, H.; Ma, Y. High Pressure Partially Ionic Phase of Water Ice. *Nat. Commun.* **2011**, *2*, 563.
(28) Sun, C. Q.; Zhang, X.; Zhou, J.; Huang, Y.; Zhou, Y.; Zheng, W. Density, Elasticity, and Stability Anomalies of Water Molecules with Fewer than Four Neighbors. *J. Phys. Chem. Lett.* **2013**, *4*, 2565.
(29) Cross, P. C.; Burnham, J.; Leighton, P. A. The Raman Spectrum and the Structure of Water. *J. Am. Chem. Soc.* **1937**, *59*, 1134.
(30) Kittel, C. *Intrduction to Solid State Physics*, 8 ed.; John Willey & Sons, Inc: New York, 2005.
(31) Zhao, M.; Zheng, W. T.; Li, J. C.; Wen, Z.; Gu, M. X.; Sun, C. Q. Atomistic Origin, Temperature Dependence, and Responsibilities of Surface Energetics: An Extended Broken-Bond Rule. *Phys. Rev. B* **2007**, *75*, 085427.
(32) Suter, M. T.; Andersson, P. U.; Pettersson, J. B. Surface Properties of Water Ice at 150−191 K Studied by Elastic Helium Scattering. *J. Chem. Phys.* **2006**, *125*, 174704.
(33) Sun, C. Q. Thermo-mechanical Behavior of Low-Dimensional Systems: The Local Bond Average Approach. *Prog. Mater Sci.* **2009**, *54*, 179.
(34) Sun, C. Q.; Pan, L. K.; Li, C. M.; Li, S. Size-Induced Acoustic Hardening and Optic Softening of Phonons in InP, CeO_2, SnO_2, CdS, Ag, and Si Nanostructures. *Phys. Rev. B* **2005**, *72*, 134301.
(35) Medcraft, C.; McNaughton, D.; Thompson, C. D.; Appadoo, D. R. T.; Bauerecker, S.; Robertson, E. G. Water Ice Nanoparticles: Size and Temperature Effects on the Mid-infrared Spectrum. *Phys. Chem. Chem. Phys.* **2013**, *15*, 3630.
(36) Gu, M. X.; Zhou, Y. C.; Sun, C. Q. Local Bond Average for the Thermally Induced Lattice Expansion. *J. Phys. Chem. B* **2008**, *112*, 7992.
(37) Kuhne, T. D.; Khaliullin, R. Z. Electronic Signature of the Instantaneous Asymmetry in the First Coordination Shell of Liquid Water. *Nat. Commun.* **2013**, *4*, 1450.
(38) Tang, Q. H.; Wang, T. C.; Shang, B. S.; Liu, F. Thermodynamic Properties and Constitutive Relations of Crystals at Finite Temperature. *Sci. China, Ser. G: Phys., Mech. Astron.* **2012**, *G 55*, 933.
(39) Su, Y. J.; Wei, H.; Gao, R. G.; Yang, Z.; Zhang, J.; Zhong, Z. H.; Zhang, Y. F. Exceptional Negative Thermal Expansion and Viscoelastic Properties of Graphene Oxide Paper. *Carbon* **2012**, *50*, 2804.
(40) Martinek, C.; Hummel, F. A. Linear Thermal Expansion of 3 Tungstates. *J. Am. Ceram. Soc.* **1968**, *51*, 227.
(41) Mary, T. A.; Evans, J. S. O.; Vogt, T.; Sleight, A. W. Negative Thermal Expansion from 0.3 to 1050 K in ZrW_2O_8. *Science* **1996**, *272*, 90.
(42) Sun, C. Q. Dominance of Broken Bonds and Nonbonding Electrons at the Nanoscale. *Nanoscale* **2010**, *2*, 1930.
(43) Lo Nostro, P.; Ninham, B. W. Hofmeister Phenomena: An Update on Ion Specificity in Biology. *Chem. Rev.* **2012**, *112*, 2286.
(44) Zhang, Y.; Cremer, P. Interactions between Macromolecules and Ions: The Hofmeister Series. *Curr. Opin. Chem. Biol.* **2006**, *10*, 658.
(45) Sun, Q. Raman Spectroscopic Study of the Effects of Dissolved NaCl on Water Structure. *Vib. Spectrosc.* **2012**, *62*, 110.
(46) Park, S.; Fayer, M. D. Hydrogen Bond Dynamics in Aqueous NaBr Solutions. *Proc. Natl. Acad. Sci. U.S.A.* **2007**, *104*, 16731.
(47) Aliotta, F.; Pochylski, M.; Ponterio, R.; Saija, F.; Salvato, G.; Vasi, C. Structure of Bulk Water from Raman Measurements of Supercooled Pure Liquid and LiCl Solutions. *Phys. Rev. B* **2012**, *86*, 134301.
(48) Park, S.; Ji, M. B.; Gaffney, K. J. Ligand Exchange Dynamics in Aqueous Solution Studied with 2DIR Spectroscopy. *J. Phys. Chem. B* **2010**, *114*, 6693.
(49) Gaffney, K. J.; Ji, M.; Odelius, M.; Park, S.; Sun, Z. H-Bond Switching and Ligand Exchange Dynamics in Aqueous Ionic Solution. *Chem. Phys. Lett.* **2011**, *504*, 1.